ResearchGate

See discussions, stats, and author profiles for this publication at: https://www.researchgate.net/publication/257934702

Mesoporous Thin Films of TiO2 on Attenuated Total Reflection Crystals. An In Situ Fourier-Transform Infrared Study of the Kinetics and Equilibrium of Adsorption and Photocatalysis...

ARTICLE *in* THE JOURNAL OF PHYSICAL CHEMISTRY C · JUNE 2013

Impact Factor: 4.77 · DOI: 10.1021/jp312334y

CITATIONS
5

READS
98

4 AUTHORS:

Federico Roncaroli
Comisión Nacional de Energía Atómica
27 PUBLICATIONS **556** CITATIONS
SEE PROFILE

Eduardo David Martínez
Comisión Nacional de Energía Atómica
9 PUBLICATIONS **71** CITATIONS
SEE PROFILE

Galo J A A Soler-Illia
National University of General San Martín
144 PUBLICATIONS **8,186** CITATIONS
SEE PROFILE

Miguel A Blesa
Comisión Nacional de Energía Atómica
230 PUBLICATIONS **4,073** CITATIONS
SEE PROFILE

Available from: Galo J A A Soler-Illia
Retrieved on: 01 February 2016

* UNKNOWN * | MPSJCA | JCA10.0.1465/W Unicode | jp-2012-12334y.3d (R3.5.i2:3995 | 2.0 alpha 39) 2012/02/08 02:21:00 | PROD-JCA1 | rq_1461456 | 6/21/2013 20:08:44 | 9 | JCA-DEFAULT

THE JOURNAL OF PHYSICAL CHEMISTRY C

Article

pubs.acs.org/JPCC

Mesoporous Thin Films of TiO_2 on Attenuated Total Reflection Crystals. An In Situ Fourier-Transform Infrared Study of the Kinetics and Equilibrium of Adsorption and Photocatalysis of Carboxylic Acids

Federico Roncaroli,*[,†,§] Eduardo D. Martínez,[‡] Galo J. A. A. Soler-Illia,[‡,§] and Miguel A. Blesa[‡,∥]

[†]Department of Condensed Matter Physics and [‡]Department of Chemistry, Centro Atómico Constituyentes, Comisión Nacional de Energía Atómica (CNEA), Buenos Aires, Argentina

[§]Department of Inorganic, Analytic and Physical Chemistry, Faculty of Exact and Natural Sciences, University of Buenos Aires, Buenos Aires, Argentina

[∥]Environmental Research and Engineering Institute, University of San Martin, San Martin, Buenos Aires, Argentina

Supporting Information

ABSTRACT: Highly organized titanium dioxide (TiO_2) mesoporous thin films were deposited directly on silicon attenuated total reflection (ATR) crystals by dip-coating, submitted to two different thermal treatments, and characterized by ellipsometric porosimetry analysis (EPA), X-ray diffraction, and electron microscopy. The kinetics and equilibrium of the adsorption of oxalic acid as well as their photocatalytic efficiency were studied in situ by Fourier transformed infrared spectroscopy (FTIR-ATR). The spectral properties and the Langmuir constants of the detected surface complexes resemble those previously found in TiO_2 Degussa P25 and anatase particulate films. The photocatalytic activity for the oxidation of oxalic acid was found to be similar to the corresponding one for Degussa P25. The kinetics of adsorption of oxalic acid follows a pseudo-first-order behavior. The pseudo-first-order rate constants show a linear relationship with the oxalic acid concentration. Adsorption (k_a) and desorption rate constants (k_d) were obtained. The k_a values were analyzed in relation to the pore and neck sizes, accessible volume, thickness, and film area. The film area affects strongly the kinetic parameters, while no clear dependence on the thickness value was observed. When the film area is taken into account, adsorption rates on mesoporous films are appreciably larger than on particulate films. Thus, enhanced adsorption rates make mesoporous films better candidates as photocatalysts. The difference is interpreted in terms of a reduced tortuosity in the ordered mesoporous films, probably due to their regular spatial order. It is also concluded that sensors and catalysts based on mesoporous films should respond faster than those based on conventional films.

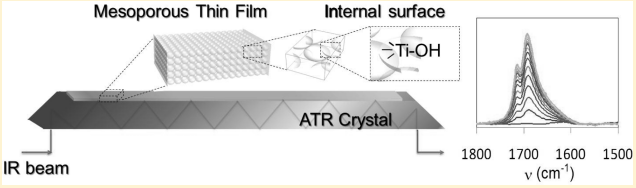

INTRODUCTION

The photocatalytic activity of titanium dioxide to oxidize organic substances dissolved in water, using O_2 as an electron acceptor, has been known for a long time.[1,2] On the other hand, with the advent of nanotechnology, a vast number of solids with different nanoarchitectures have been synthesized, some of them with novel properties related in part to their large specific surface area.[3−5] In this way, mesoporous TiO_2 thin films have attracted attention as potential heterogeneous photocatalysts,[6] sensors,[7] supports for catalysts,[8] and enzymes[9] and active material for dye-sensitized solar cells.[10] To be able to understand and to design materials with such properties and, eventually, with optimum performance, it is necessary to have a deep knowledge of the basic processes that take place on the surface.[4−8,10,11] Not only the catalyzed reaction is important but also the rate and equilibrium for adsorption.

This is in line with some previous reports from our group on the adsorption of different carboxylic acids on TiO_2 Degussa P25 and anatase films.[12−14] In these cases, as in the present report, attenuated total reflection Fourier transform infrared spectroscopy (ATR-FTIR) was used to follow the evolution of the surface complexes with time and concentration. This technique is particularly useful since it is highly selective for the species present on the solid−solution interface; the solutes present in bulk do not usually interfere.[15] Moreover, FTIR spectroscopy offers the possibility to identify different surface complexes using their characteristic frequencies as fingerprints.[16−18] In this way, several studies on the equilibrium of adsorption of different carboxylic acids have been reported. Spectra at different concentrations can be analyzed by singular value decomposition (SVD) affording the spectra and Langmuir constants of the different surface complexes.[15] The information thus obtained is complementary to the large number of data obtained *in batch*.[19] However, this last

Received: December 14, 2012
Revised: May 27, 2013

 © XXXX American Chemical Society dx.doi.org/10.1021/jp312334y | J. Phys. Chem. C XXXX, XXX, XXX−XXX

technique does not give information on the nature of the surface complexes. FTIR-ATR has also been used successfully to identify the different surface complexes generated during the photolysis of oxalic acid on TiO_2.[20]

In our recent paper on different anatase particulate films, it was shown that particle size, thickness, and film area deeply influence adsorption kinetics.[12,13] However, the influence of the pore size and the accessible volume (porosity) was not studied to our best knowledge. Organized mesoporous titania thin films (MTTFs) with highly controlled pore volume, size, and geometry constitute an excellent testing system, due to the possibility of a systematic fine-tuning of these features in a reproducible way. Although in the last years several publications have presented the photocatalytic performance of MTTFs, no thorough description and analysis of the basic adsorption and desorption processes taking place has been so far reported.

In the present report, the kinetics and equilibrium of adsorption of oxalic acid on highly organized mesoporous TiO_2 thin films are studied. The films were deposited on Si ATR crystals through dip coating and subsequently heated at different temperatures, to consolidate the structure of the films, eliminate the template, and lead to wall crystallization. This thermal treatment did not appreciably modify the optical properties of the crystals, which remained suitable for ATR spectroscopy. As far as we know, this procedure has not been reported on ATR crystals so far. This in situ analysis permits us to understand the adsorption processes in an environment close to the actual operation situation of a photoactive coating. The films thus obtained were studied through ellipso-porosimetry analysis (EPA) X-ray diffraction and electron microscopy. EPA affords the pore and neck size distributions of the films, as well as the thickness and the accessible volume. The influence of these parameters on the kinetic and equilibrium of the adsorption of oxalic acid as well as the photocatalytic properties were studied.

EXPERIMENTAL METHODS

Oxalic Acid Dihydrate. Oxalic acid dihydrate (Merck) was analytical grade and used without further purification. Deionized water was doubly distilled from a quartz apparatus. Diluted NaOH or HCl solutions (Merck) were used to adjust the pH at 4.0, and NaCl (Merck) was used to control ionic strength at 0.01 M. All the other chemicals were analytical grade (Aldrich or Merck) and used as purchased.

Mesoporous Titania Films. Mesoporous titania films were synthesized following the sol−gel procedures described by Crepaldi et al.[4,5,21] Poly(ethylene oxide)-based surfactants such as Pluronics F127 ($PEO_{106}PPO_{70}PEO_{106}$) or Brij 58 ($C_{16}H_{33}PEO_{20}$) were added to an ethanol solution of titanium tetrachloride ($TiCl_4$). Water was added to the sol, satisfying the final molar relation of the sol $TiCl_4$:EtOH:(F127/Brij58):H_2O equal to 1:40:(0.005/0.05):10.

The ATR crystals, previously washed with acetone, ethanol, and water and dried at 60 °C, were dipped into the sol at 35 °C and extracted at a constant withdrawal rate of 3 mm s^{-1} for the Brij58 titania films (TB) and 2 mm s^{-1} for the F127 titania films (TF); the relative humidity (RH) of the dip-coater chamber was set to 35%. After the coating process was complete, the film deposited on the lateral and reverse sides of the ATR crystals was removed, and the one-faced films were placed in a closed chamber at 50% RH for 24 h for the stabilization of the mesostructure.[21,22] The films were then submitted to a thermal treatment of 24 h at 60 °C and 24 h at 130 °C, allowing for the condensation reactions to proceed, and finally calcined at 350 °C for the removal of the polymeric surfactant. A different thermal treatment, referred as STT (short thermal treatment), was employed in the synthesis of additional films. In this treatment, the temperatures were the same as before, but the residence times in each stage were reduced from 24 h to 30 min. This fast procedure limits the condensation reactions of the Ti(IV) species, and the final film possesses a higher content of micropores with respect to the ones resulting from the standard procedure.[23] In our previous reports, particulate films were obtained upon gentle drying out of a colloidal water suspension spread on the ATR crystals.[12,13]

Electron Microscopy Analysis. Electron microscopy analysis was performed to reveal the porous structure of the templated and particulate mesoporous thin films. The surface was analyzed with the use of a field emission scanning electron microscope (FE-SEM) (Carl Zeiss, Supra 40). Transmission electron microscopy (TEM) analysis was performed on a Philips EM 301 operated with tension below 100 kV. The TEM samples were prepared by scratching the films and depositing the fragments over an ethanol drop placed on a carbon-coated copper grid.

Grazing Incidence X-ray Diffraction. Data were acquired on a Panalytical Empyrean diffractometer utilizing Cu K_α radiation. The diffractometer was configured on the incident beam side with a parallel beam mirror and a 1/2 degree divergence slit. On the diffracted beam side, a parallel plate collimator was used along with 0.04 rad Soller slits. Detection was via a Pixel 3D. The sample was mounted on a Eulerian cradle and was aligned according to standard procedures.

Ellipsometric Measurements (EPAs). EPAs were performed in commercial SOPRA GES5A equipment with the use of a microspot optical configuration at an incidence angle of 75°. Before the measurements, the films were washed with acetone and ethanol and dried at 130 °C. For the accurate determination of the thickness, the samples were measured on five different points, and the ATR silicon substrate was measured independently for the proper fitness of the optical data. The EPA measurements were performed using a closed chamber inside which the relative humidity (RH) can be set through the control of N_2 and water vapor fluxes. EPA measurements at different RH values were performed. The data obtained were analyzed by the use of Winelli II software proposing a model for the dielectric function based on a Cauchy dispersion relation and a Lorentz oscillator for the absorption of the titania in the UV region. The fitting procedure allowed the accurate determination of the optical constants and the thickness of the films at each RH, making a water adsorption isotherm from which the total accessible volume can be attained.[24] The size distribution of pores and necks was determined by the analysis of the adsorption and desorption branches of the isotherm, respectively, according to the Kelvin equation, which relates the relative pressure of the adsorbate (water in our case) and the change in the volume of water adsorbed.[25] A spherical geometry of pores and a wetting angle of 30° for the H_2O−TiO_2 interface were assumed. The results obtained by this simplified model are sufficiently accurate for the description of the samples characteristics that determine their catalytic properties. Error values in pore and neck sizes were taken as the standard deviation from the Gaussian fits (Supporting Information Figures SI 3, SI 4, and SI 5); the error in thickness arises from statistical fluctuation (~4%) of measurements performed on different points of the samples.

dx.doi.org/10.1021/jp312334y | J. Phys. Chem. C XXXX, XXX, XXX−XXX

ATR-FTIR Measurements. The measurements were performed in a Nicolet Magna IR 560 spectrometer equipped with a MCT-A detector cooled by liquid N_2. ATR cells were mounted on a Spectratech ARK accessory. The spectrometer and the last accessory were purged with dry air generated in a Whatman FTIR purge gas generator.

Kinetics and Equilibrium Studies. Studies were performed with a horizontal ATR flow cell Spectratech ARK 0056-303. A 12 reflection trapezoidal Si ATR crystal (0.3 × 7.2 × 1.0 cm, from Medway Optics), coated in the smaller face (7.2 × 1.0 cm), with the thin TiO_2 film was placed inside. The procedures to obtain the isotherms and the kinetic traces were similar to the ones previously employed for particulate films and reported in the literature.[12,13] The ATR flow cell was connected by two Teflon tubes to a 500 mL cylindrical glass cell, which was thermostatically set at 25.0 °C and deaerated by continuous slow N_2 bubbling. A Hewlett-Packard 89052B peristaltic pump was used to flow the solution from the glass cell through the ATR cell and back to the glass cell. The flow of the peristaltic pump was 8.1 mL/min. The coated crystal was placed in the ATR flow cell, and at least 200 mL of water was flowed through it to remove impurities and equilibrate the surface, before connecting the glass cell that contained 300 mL of NaCl solution (0.01 M) at pH 4.0. After equilibration, the IR spectrum of this NaCl solution was taken as a blank experiment and was subtracted to the spectra of all the solutions.

To obtain the isotherms, aliquots of increasing amounts of oxalic acid of two solutions of 2.5×10^{-3} M (for lower concentrations) and 0.054 M (for final higher concentrations) with pH 4.0 (without NaCl for the ionic strength) were added to the glass cell. Equilibrium conditions were considered to be met when the spectra showed no more appreciable changes, which took from two hours (for the lowest concentrations) until 15 min (for the highest ones). The spectra obtained in equilibrium with different oxalic acid concentrations were analyzed through SVD-Global analysis as previously reported for oxalic acid and several other ligands.[15−18] A Langmuirian model was employed for each of the surface complexes. At least 11 oxalic acid concentrations were measured in the range 4×10^{-7}−10^{-3} M.

In a typical kinetic experiment, an oxalic acid solution 2.5×10^{-3} M with pH 4.0 (without NaCl for the ionic strength) was prepared. The ATR cell was emptied; aliquots of the acid solution were added to the glass cell (0.01 M NaCl, pH 4.0, T = 25.0 °C); and after homogenization the solution was flowed through the cell. As soon as it reached the ATR cell spectra acquisition was started. Spectra were recorded from 1500 to 2000 cm^{-1} (to avoid the interference of Si absorption bands), usually every 3 min (250 scans, resolution 2 cm^{-1}). The acquisition of each spectrum lasted 160 s. The time when acquisition started was taken as the time of the spectrum. When the spectra showed no more appreciable changes, the ATR cell was emptied, and the film was washed with distilled water until signals of oxalic acid were no longer observed. Then a new aliquot of the carboxylic acid solution was added to the glass cell, and the experiment was restarted following the same procedure. This allowed for studying the adsorption kinetics in the concentration range 4×10^{-7}−4×10^{-6} M, and in some cases the concentration range was broader. The successive spectra of each experiment were baseline corrected, using the spline mode of the OMNIC 5.0 software. The area of the spectrum (1750−1600 cm^{-1}) as a function of the time was fitted to an exponential equation with Origin Lab software, i.e., $A = A_{eq}(1 - e^{-k_1 t})$, where A is the absorbance at a certain wavenuber at a time t, A_{eq} the corresponding equilibrium value, and k_1 the pseudo-first-order rate constant. The analyzed interval of time was three half-lives of the adsorption process or longer. Linear plots, slopes, intercepts, and the corresponding error were calculated using Microsoft Excel.

Photolysis. For these experiments, a homemade flow ATR cell was used. The cell is basically similar to the flow cell described above for the kinetic and equilibrium experiments, but in this case the plate of aluminum that holds the ATR crystal was replaced by an acrylic window transparent to UV light (14.6 cm × 6.34 cm × 1.02 cm, 50% of transmittance at 375 nm) (see picture in the Supporting Information). The cell was illuminated from above with a Phillips 15 W tubular lamp (355 nm). The power on the surface of the cell was 0.2 mW cm^{-2}. Although the cell is designed to carry out experiments under flow conditions, the flow was stopped during illumination. A solution of 0.1 mM oxalic acid, pH 4.0, saturated in oxygen was flowed through the cell. When equilibrium was reached, i.e., spectral changes were no longer observed, the flow was stopped, and the UV light was turned on. The spectral areas were fitted accurately with an exponential function of the irradiation time, using the Origin program. The same program afforded the errors of the parameters.

Estimation of Pore and Neck Sizes, Film Areas, and Accessible Volumes of the Particulate Films. A simple cubic packing with spheres in the vertices of a cube was assumed. In a compact model (i.e., bcc or fcc) the spherical particles would be in the vertices of a tetrahedron, and this last model would afford a minimum value for the pore and neck sizes. According to the SEM pictures, the particulate films show appreciable disorder; for this reason the simple cubic packing was employed, which would be an intermediate situation between a compact packing and a fully disordered one (see Supporting Information Figure SI 6). Since the pores are not spherical and not monodisperse, the pore size of Degussa P25 and Kemira S230 films was approximated as equal to the particle radius as suggested from the FE-SEM images (see Supporting Information Figure SI 6). The particle radius was assumed as half the crystalline domain obtained from the broadening of the (101) peak of anatase using the Scherrer formula.[13] However this method may overweigh the larger particles, when compared with the FE-SEM technique, from which a particle size between 15 and 35 nm for Degussa P25 was obtained (see Supporting Information Figure SI 6). A value for the error of particle radius was estimated as 2 nm for Kemira S230 and 6 nm for Degussa P25.

The neck sizes for the same films were estimated employing the same model. For the actual calculation, the section of the neck (surface) was taken as the surface left between four adjacent circles of radius equal to the particle radius. Since the neck is not cylindrical, an *apparent* radius was calculated from this surface that equals (see Supporting Information Figure SI 7)

$$\text{Neck radius} = [(4 - \pi)/\pi]^{1/2} \times \text{particle radius} \quad (1)$$

A value for the errors in the neck radii were taken as 1 nm for Kermira S230 and 3 nm for Degussa P25.

Film areas of the particulate films were calculated from the TiO_2 load and the BET area.

Film areas of the mesoporous films were estimated assuming spherical pores (i.e., with the pore sizes, the area of the pores was calculated, and with the accessible volume and the

dx.doi.org/10.1021/jp312334y | J. Phys. Chem. C XXXX, XXX, XXX−XXX

geometrical volume of the film, the number of the pores was calculated).

$$\text{Film Area} = 3 \times \text{geometrical area} \times \text{thickness} \times \text{accessible volume/Pore radius} \quad (2)$$

The geometrical area is the area of the ATR crystal covered by the TiO_2 film, i.e., 7.2 cm^2.

To calculate the accessible volume (V_{max}, %) of the Degussa P25 and Kemira S230 films, the geometrical volume and the occupied volume are needed. The geometrical volume was 7.2 cm ×1.0 cm × thickness (measured by ellipsometry and AFM). The occupied volume was taken by dividing the film mass (0.12 mg of Degussa P25 and 0.13 mg of Kemira S230) by the density of anatase (3.89 g cm^{-3}). Errors were propagated using the equations mentioned above.

RESULTS AND DISCUSSION

Characterization. TiO_2 mesoporous thin films using two different templates were directly deposited by dip-coating on Si ATR crystals. Silicon was chosen due to its suitable thermal, mechanical, and chemical properties that allow for the (low temperature) crystallization of titania[26,27] required for good photocatalytic performance.[4,5] Grazing incidence X-ray diffractograms confirmed the presence of the anatase phase in the films (see Supporting Information, Figure SI 8). Silicon is also a convenient substrate for ellipsometric characterization (EPA). The characterization of the mesoporous films through EPA can be found in the Supporting Information. Two different thermal treatments were employed, 350 and 450 °C. They were also studied after and before they were brought in contact with the oxalic acid solutions. The results are summarized in Table 1.

Ellipso-porosimetry experiments reveal that the TF films display higher values of pore and neck sizes, thickness, and accessible volume than TB films (see Supporting Information Figures SI 3 and 4 and Table 1). The films treated at 450 °C show a slight decrease in the thickness and an increase in the pore and neck sizes as compared to films treated at 350 °C due to further condensation of the inorganic matrix, in agreement with previous reports.[22,28,29] The accessible volumes do not show a clear correlation with the thermal treatment in these cases. The areas of these films were estimated using eq 2. According to this model the areas were close to 0.03 m^2 for all the films except for the Degussa P25 film (0.006 m^2). This is in agreement with the previous report of the BET area of the TF film[21] of 150 m^2 g^{-1}, considering a density of 2.1 g cm^{-3} as suggested from XRR measurements reported elsewere.[30] The Kemira S230 film shows a similar area to the mesoporous films (0.031 m^2, see Table 1 and Supporting Information Table SI 2).

More interesting is the effect on the films put in contact with the oxalic acid solutions: the pore and neck sizes increase in all cases, which can be interpreted in terms of some extent of dissolution of the most external layers of the exposed surface of TiO_2; this behavior has been reported for strong Ti(IV) complexing agents such as TIRON in contact with MTTF.[31] Attempts to measure the pore and neck sizes of the particulate films through EPA failed due to high dispersion of these films.

Electron microscopy reveals the long-range ordered structure of the MTTF. In Figure 1(a) a FE-SEM image of the surface of a TF film deposited on a silicon substrate is presented, while in Figures 1(b) and (c) TEM images of TF and TB treated at 350 °C are displayed.

Table 1. Physical Properties and Kinetic and Thermodynamic Data for the Studied Films

	thermal treatment (°C)	necks (nm)[a]	pores (nm)[a]	thickness (nm)[a]	V_{max} (%)[a]	film area (m^2)[b]	k_a (M^{-1} s^{-1})[c]	k_d (s^{-1})[c]	$\log(k_a/k_d)$	log $K_L(I)$[d]	k_{ph} (s^{-1})[e]
S 230[f]		2 ± 1	4 ± 2	70 ± 20	33 ± 9	0.031 ± 2 × 10^{-3}	450 ± 20	2 ± 1 × 10^{-4}	6.7−6.2	6.18	
TB	350	2.8 ± 0.3 (2.8 ± 0.3)	3.9 ± 0.7 (3.9 ± 0.6)	131 ± 5 (131 ± 5)	45.0 ± 0.1 (42.4 ± 0.1)	0.032 ± 7 × 10^{-3}	1080 ± 60	ca. 2 × 10^{-4}		6.7	1.8 ± 0.7 × 10^{-3}
	450	3.2 ± 0.3 (3.2 ± 0.4)	4.5 ± 0.9 (4.7 ± 0.7)	128 ± 5 (123 ± 4)	39.6 ± 0.1 (41.2 ± 0.1)	0.024 ± 7 × 10^{-3}	1050 ± 70	4 ± 1 × 10^{-4}	6.6−6.3	6.4	1.7 ± 0.6 × 10^{-3}
TF	350	3.2 ± 0.4 (3.5 ± 0.4)	5.0 ± 0.8 (5.1 ± 0.8)	170 ± 6 (171 ± 6)	46.9 ± 0.1 (45.4 ± 0.1)	0.034 ± 7 × 10^{-3}	1320 ± 70	ca. 1 × 10^{-4}		6.6	1.4 ± 0.1 × 10^{-3}
	450	3.8 ± 0.5 (4.0 ± 0.6)	5.6 ± 0.9 (6.0 ± 0.9)	168 ± 6 (166 ± 6)	50.1 ± 0.1 (48.0 ± 0.1)	0.030 ± 7 × 10^{-3}	1260 ± 60	4 ± 2 × 10^{-4}	6.8−6.3	6.7	1.1 ± 0.2 × 10^{-3}
TF STT	350	3.9 ± 0.9	5.6 ± 0.9	170 ± 6	46.6 ± 0.1	0.031 ± 7 × 10^{-3}	1310 ± 10	1.6 ± 0.8 × 10^{-4}	7.2−6.7		1.0 ± 0.4 × 10^{-3}
P 25[f]		10 ± 3	19 ± 6	170 ± 20	75 ± 9	0.0060 ± 5 × 10^{-4}	3300 ± 200	2.7 ± 0.2 × 10^{-3}	6.1−6.0	6.1−6.6	2.4 ± 0.4 × 10^{-3}

[a]Data obtained from ellipso-porosimetry (V_{max} is accessible volume), except for the particulate films. [b]Estimated from pore size thickness and accessible volume (see eq 2 Experimental section), except for the particulate films which were calculated from the BET area and film load (see Supporting Information Table SI 2). [c]From eq 3. [d]From SVD analysis, see Figure 2 and Supporting Information. [e]Observed rate constant for the photolysis of oxalic acid; see Experimental section and Supporting Information. [f]From ref 13, for the neck, pore size, and accessible volume, see eq 1 and the Experimental section. Film thicknesses were extracted from ellipsometry at 0% RH and supported by AFM and FE-SEM images. For error estimation see the Experimental section.

dx.doi.org/10.1021/jp312334y | J. Phys. Chem. C XXXX, XXX, XXX−XXX

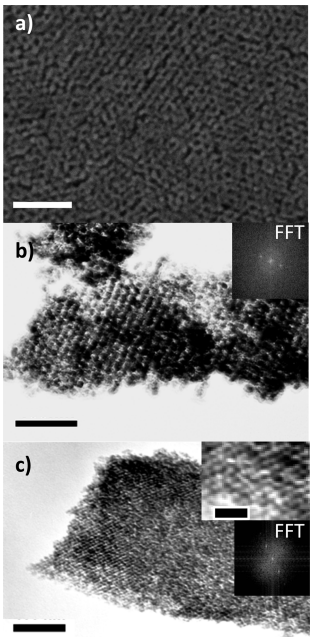

Figure 1. (a) FE-SEM and (b) TEM images of TiO_2-F127 deposited on the silicon substrate and treated at 350 °C (scale bar: 100 nm). Inset: fast Fourier transform (FFT) showing the ordered structure of the porous framework. (c) TEM image of TiO_2-Br58 on silicon calcined at 350 °C (scale bar: 100 nm, inset: 25 nm).

Equilibrium. Figure 2 shows the FTIR spectra of different oxalic acid solutions in equilibrium with a TB film (350 °C). The strong absorption of Si limited the accessible spectrum to wavenumbers higher than 1500 cm^{-1}. The spectra at different concentrations were analyzed by SVD global analysis. Three spectral components were necessary to simulate the experimental data using Langmuirian isotherms for each one. The Langmuir constants were 4.8×10^6, 4.0×10^4, and 8.6×10^2 M^{-1} at pH 4.0 for the three spectral components. Similar values were obtained for TB treated at 450 °C and for TF at both temperatures (Supporting Information Figures SI 9 and 10). These data are in good agreement with several reports on Degussa P25 films and other anatase particulate films.[12,13,15,17] Thus, the Langmuir constants for the three surface complexes on TiO_2 Degussa P25 are in the range $1.2–4.0 \times 10^6$ M^{-1}, $0.3–4.0 \times 10^5$ M^{-1}, and $1.0–3.2 \times 10^3$ M^{-1}.[15] In the Supporting Information (Table SI 1), the Langmuir constants for the three spectral components of each film are presented, together with the position of the IR absorption bands and the assignment based on previous reports. The spectra of the surface complexes detected on the MTTF are similar to the ones reported for TiO_2 Degussa P25[17,18] (see Supporting Information Table SI 1). It is interesting to note that the Langmuir constants for the most stable surface complex, i.e., $K_L(I)$, are slightly higher for the mesoporous films than for the particulate films. A discussion of the structure of these surface complexes has been proposed based on theoretical calculations.[20]

The IR spectra of a 0.1 mM oxalic solution acid in equilibrium with different MTTFs display similar absorbance values (see Supporting Information Figure SI 12). However, the absorbance of a Degussa P25 film of the same area is appreciably lower. The number of exchangeable sites per nanometer should be the same in all the anatase samples (surface site density for TiO_2 Degussa P25 has been reported to be 1.79 sites nm^{-2}).[32] In contrast, the access of the adsorbate to these sites must be different since the MTTFs have a highly ordered pore distribution and particulate films are disordered. This idea will be discussed later in terms of the tortousity of the films.

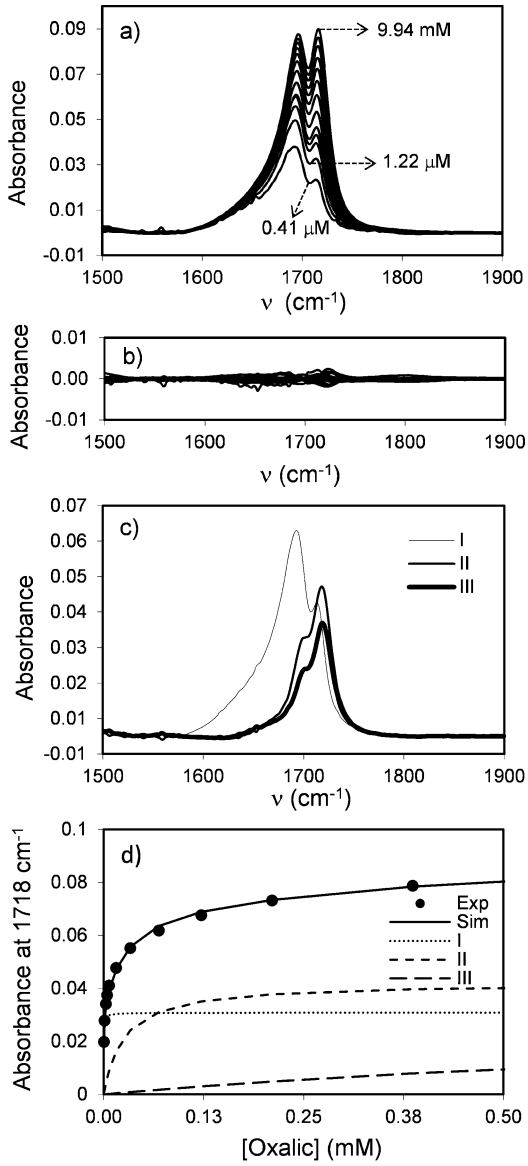

Figure 2. (a) Spectra of adsorbed oxalic acid at different solution concentrations in equilibrium with a film TB (350 °C) (concentration range $4 \times 10^{-7}–10^{-3}$ M, pH 4.0, I = 0.01 M, T = 25.0 °C). (b) Residuals of the fit. (c) Spectra of the three detected surface complexes obtained from SVD analysis. (d) Absorbance at 1718 cm^{-1}. Full circles are experimental data, dashed lines correspond to the contribution of each surface complex, solid line is the sum of the three components. $K_L(I) = 4.8 \times 10^6$ M^{-1}, $K_L(II) = 4.0 \times 10^4$ M^{-1}, $K_L(III) = 8.6 \times 10^2$ M^{-1}.

Kinetics. The kinetics of the adsorption of several carboxylic acids on TiO_2 films, particularly oxalic, can be fitted with reasonable accuracy by an exponential function, i.e., $A = A_{eq}(1 - e^{-k_1 t})$, where A is the absorbance at a certain wavenumber and time t, A_{eq} the corresponding equilibrium value, and k_1 the pseudo-first-order rate constant.[33] This pseudo-first-order model has been employed in an empirical way for a long time to study the adsorption kinetics of a wide variety of ions and organic molecules on different adsorbents.[33] Recently theoretical grounds for this use have been established.[34–38] From the fitting (see Figure 3 for TB (350 °C)), pseudo-first-order rate constants were obtained (k_1). In agreement with

dx.doi.org/10.1021/jp312334y | J. Phys. Chem. C XXXX, XXX, XXX–XXX

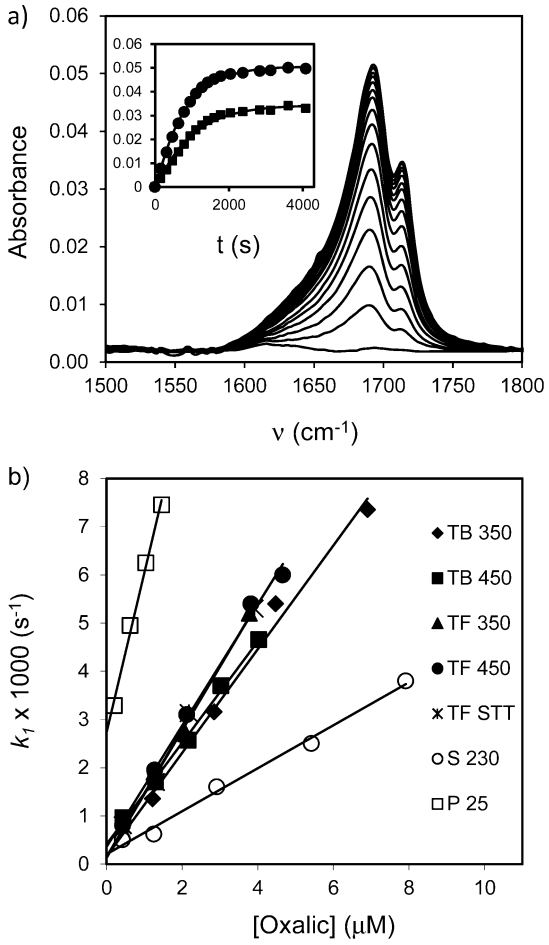

Figure 3. (a) Spectral changes observed during the adsorption of oxalic acid on TB (350 °C). Concentration 1.2×10^{-6} M, pH 4.0, I = 0.01 M, T = 25.0 °C. Inset: kinetic traces at different wavenumbers (circles, 1691 cm^{-1}) $k_1 = 1.3 \times 10^{-3}$ ($\pm 10^{-4}$) s^{-1} and (squares, 1714 cm^{-1}) $k_1 = 1.1 \times 10^{-3}$ ($\pm 10^{-4}$) s^{-1}. (b) Plots of pseudo-first-order rate constants (k_1) vs oxalic acid concentration for different films under study. pH 4.0, T = 25.0 °C, I = 0.01 M (NaCl). Values of the slopes and intercepts are listed in the Table 1. Data of Degussa P25 and Kemira S230 were extracted from ref 13.

previous reports, these parameters depend linearly on the solution concentration of adsorbate (see eq 3 and Figure 3).[12,13] The slopes of these plots are interpreted in terms of the rate constant for adsorption (k_a) and the intercept in terms of the dissociation rate constant (k_d). The kinetic data for the studied mesoporous thin films are summarized in Table 1. Information from previous reports on the particulate films from Degussa P25 and Kemira S230 is also included for comparison.[12,13]

$$k_1 = k_a[\mathrm{L}] + k_d \qquad (3)$$

The quotient k_a/k_d is a good approximation to the Langmuir constant K_L.[12,13] We had already shown that, when more than one surface complexes or adsorption modes are present, like with oxalic acid, they display a single adsorption process (k_a) because the intraparticle diffusion controls the overall adsorption rate and all surface complexes are equilibrated between them at all times.[12,13] The desorption constant we measure (k_d) corresponds to the release of the most stable surface complex (I), hence k_a/k_d is approximately $K_L(I)$ (see Supporting Information Table SI 1).[12,13,16]

In a previous report by our group a biexponential process was observed for gallic acid adsorption on particulate Degussa P-25 films in a batch cell.[14] The present results suggest that the second exponential trace, whatever its origin may be, is a characteristic associated with the behavior of gallic acid.[14]

The kinetic parameters for the STT film, prepared with a special thermal treatment described in the Experimental section,[23] were very similar to the ones of standard TF.

An open question from our last reports[12,13] was whether the pore and neck sizes, or the film area and thickness, determine the rates for adsorption and desorption. All the above-mentioned parameters together with the kinetic data for all the studied films are shown in Table 1. A linear correlation is shown in Figure 4, for k_a vs neck radius. In the Supporting

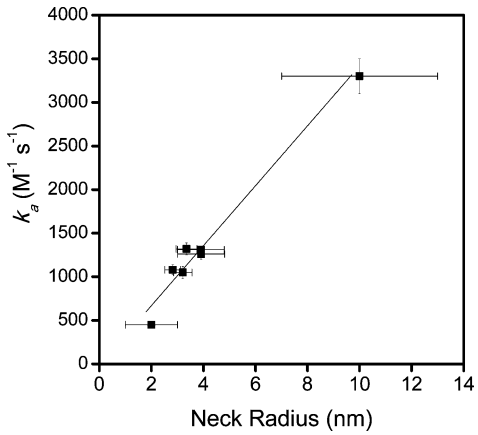

Figure 4. Plot of the adsorption (k_a) rate constant vs the radius of the necks for the films described in the Experimental section and Table 1. Extreme points correspond to Degussa P25 and Kemira S230 films.

Information (Figures SI 13 and SI 14) plots of the rate constant for adsorption on the films vs different parameters, i.e., pore size, accessible volume, and thickness, are shown. In most cases similar linear correlations are observed. In fact, pore and neck radii and accessible volume are correlated.

No correlation of k_a with the thickness of the film is observed (see Supporting Information Figure SI 14). The intraparticle diffusion model has been most extensively applied to adsorption on particles. This model predicts a linear dependence of k_1 with $(1/r^2)$ (where r is the particle radius).[36] On the other hand, a very good correlation has been observed between k_a and the inverse of the film area with particulate films.[12,13] In Figure 5, data on these last films are also shown for comparison, and Table SI 3 (Supporting Information) gives the detailed data. The points corresponding to the mesoporous films fall outside the correlation (black circles) and show k_a values higher than expected according to their surface area. We attribute this behavior to a lower tortuosity in the mesoporous films due to their highly ordered pores. This is certainly not the case for particulate films (see FE-SEM Figure 1 and Supporting Information Figures SI 6).

To analyze the influence of the pore size (and, hence, the neck size and accessible volume, since they are correlated), the rate constants for adsorption (k_a) were normalized to 0.03 m^2; in this way surface area-independent k_a° values are obtained (i.e., $k_a^\circ = k_a \times$ film area (m^2)/0.03 m^2). A plot of k_a° vs pore radius is shown in Figure 6. Data for particulate films are also shown. Upon increasing the pore radius, a saturation behavior is observed (see dashed line); i.e., for pore radius higher than

dx.doi.org/10.1021/jp312334y | J. Phys. Chem. C XXXX, XXX, XXX−XXX

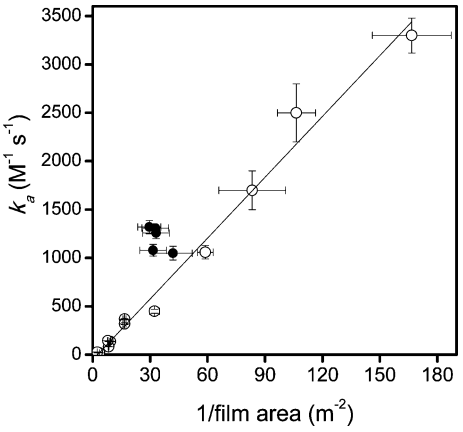

Figure 5. Plot of the adsorption rate constant vs the inverse of the surface area. Open circles correspond to values reported in ref 13. (Values reproduced in Supporting Information Table SI 2.) Black circles correspond to the mesoporous thin films.

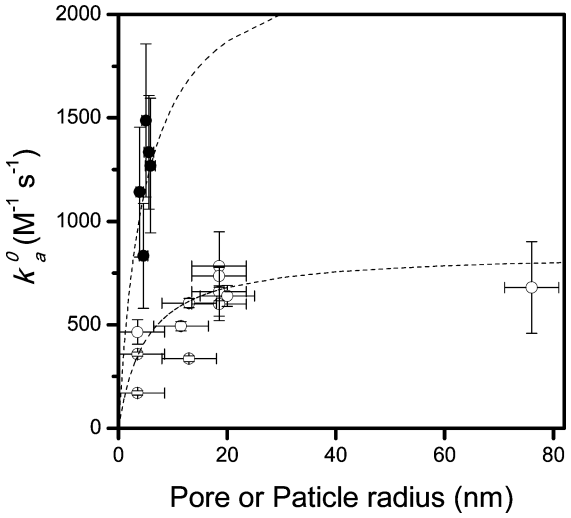

Figure 6. Plot of the rate constant of adsorption normalized to a film area equal to 0.03 m^2 (k_a^o) vs pore radius (mesoporous films) or particle radius (particulate films). Black circles correspond to the mesoporous films (Table 1), and open circles correspond to particulate films from ref 13. (Values reproduced in Supporting Information Table SI 3.)

ca. 20 nm k_a^o becomes independent of the pore radius (see Figure 6). A similar result has already been reported.[39] It is concluded that when the adsorbate is small compared with the neck and/or pore radius these parameters do not control any longer the rate of adsorption. As explained, mesoporous films of similar pore radius show higher k_a^o values due to decreased tortuosity. The dotted line shows that the expected saturation effect is lower for the mesoporous films. The same reasoning would predict that the adsorbate does not diffuse through pores with radius smaller than a critical value, probably comparable to the molecular size. In agreement, we have previously shown that the dependence of both k_a and k_d on the molecular size for the adsorption of carboxylic acids on Degussa P25 films[12] is modest for small molecules, but the larger molecules, EDTA and TTHA acids (EDTA = ethylenediaminetetraacetate and TTHA = triethylenetetramine-*N*,*N*,*N*′,*N*″,*N*‴,*N*‴-hexaacetate), show strongly reduced values of k_a and k_d.[12]

Photocatalysis. A homemade ATR cell (see Supporting Information Figure SI 15) was used to compare the photocatalytic efficiency for the oxidation of oxalic acid of the different films. The studies were not done under flow conditions. Such experiments will be discussed in a forthcoming report. The FTIR-ATR spectral changes of adsorbed oxalic acid on TB (350 °C) upon illumination can be observed in Supporting Information Figure SI 16. Similar spectral changes were observed for the other films. They resemble the changes observed during desorption through washing with water or an aqueous solution. The band around 1716 cm^{-1} decays faster than the band located at 1693 cm^{-1}. This can be interpreted in terms of a faster depletion of the complexes II and III from the surface (see Supporting Information Table SI 1). This has also been observed with particulate films.[20] The photolysis rate constants (k_{ph}) can be observed in Table 1. The conclusion is that all MTTFs show values of k_{ph} slightly lower than Degussa P25 (cf. ref 40). Although MTTFs have highly ordered and accessible pores, their crystalline domains of the anatase phase are around 10 nm (see Supporting Information Figure SI 8), significantly smaller than the 37 nm (see Supporting Information Table SI 2) for Degussa P25, this parameter being determinant of good photocatalytic efficiency.[4,28]

CONCLUSIONS

Mesoporous films attract much attention as potentially powerful catalysts, and the development of a method that permits the structural characterization of the film alongside with the measurement of their catalytic properties is valuable. We have shown that it is possible to grow mesoporous TiO_2 thin films with organized porosity of controlled size, obtained from template precursors, directly on ATR crystals suitable for FTIR. The physical parameters of these films can be controlled with high accuracy and reproducibility, and a narrow (approximately monodisperse) distribution of pore sizes can be achieved. Film thickness and porosity can be tuned by means of the withdrawal rate in the dip-coating process and the proper election of the templating agent, respectively. Parameters like pore and neck size, accessible volume, and thickness of the mesoporous films can be measured by ellipso-porosimetry (EPA). The FTIR-ATR spectral measurements demonstrate that the Si substrate maintains its optical quality as ATR crystal, even after the thermal treatment. Through this spectroscopy, it was possible to measure the surface affinity (isotherms) and the kinetics of surface evolution, both in the dark (adsorption kinetics) and under light (photocatalysis).

The kinetics of adsorption of oxalic acid follows a pseudo-first-order behavior. The pseudo-first-order rate constant shows a linear relationship with oxalic acid concentration. From the slope and the intercept, the adsorption rate constant (k_a) and the desorption rate (k_d) constant were obtained, respectively. k_a values were analyzed in relation to the parameters determined by EPA, namely, pore and neck sizes, accessible volume, thickness, and film surface. No evidence was found to show a clear dependence of the kinetic parameters with the film thickness; in contrast, the film area was found to play the determining role. When the film area is taken into account, the mesoporous films show appreciable larger kinetic parameters than particulate films. The difference is interpreted in terms of a reduced tortuosity in the mesoporous films, probably due to their higher order. In this way, these films are very suitable to support catalyst and be employed as sensors, where diffusion through the pores is usually a determining factor.

We have prepared TiO_2 films, but in principle other metal oxides and related materials can be studied, such as zeolites and even nanocomposites or immobilized enzymes. Also, Ge or even ZnSe can substitute for the Si substrate, thus avoiding the

dx.doi.org/10.1021/jp312334y | J. Phys. Chem. C XXXX, XXX, XXX−XXX

interference due to the Si strong absorption at wavenumbers below 1500 cm^{-1}.

In summary, the proposed method permits us to correlate catalytic activity (measuring the time evolution of the composition of the interface) with physical parameters, like pore and neck size, accessible volume, area of the film, and thickness (measured by EPA), in the same sample.

■ ASSOCIATED CONTENT

Supporting Information

Experimental details, EPA measurements, XRD of a mesoporous film, FESEM picture of particulate and mesoporous film, isotherms, table on kinetic and thermodynamic data for the studied films, FTI-ATR spectroscopic table of the studied films; plots of adsorption rate constant vs pore radius, accessible volume and thickness; photochemical data, and a model to explain the effect of the film thickness on the adsorption rate constant. This material is available free of charge via the Internet at http://pubs.acs.org.

■ AUTHOR INFORMATION

Corresponding Author

*E-mail: roncaroli@cnea.gov.ar. Tel.: (0054-11)-6772-7100.

Notes

The authors declare no competing financial interest.

■ ACKNOWLEDGMENTS

This project was supported by the National Research Council of Argentina (CONICET), ANPCyT (PICT 1848 and PAE-37063-PME-2006-00038), and the National Commission for Atomic Energy (CNEA-Argentina). M.A.B. is a Senior Researcher in CNEA and Professsor at UNSAM; GJAASI is CONICET staff member; FR was postdoctoral fellow of CONICET; and EDM is a doctoral fellow of CONICET.

■ REFERENCES

(1) Malato, S.; Fernández-Ibáñez, P.; Maldonado, M. I.; Blanco, J.; Gernjak, W. Decontamination and Disinfection of Water by Solar Photocatalysis: Recent Overview and Trends. *Catal. Today* **2009**, *147*, 1−59.

(2) Chen, X.; Mao, S. S. Titanium Dioxide Nanomaterials: Synthesis, Properties, Modifications, and Applications. *Chem. Rev.* **2007**, *107*, 2891−2959.

(3) Cao, G. *Nanostructures & Nanomaterials, Synthesis, Properties and Applications*, 1st ed.; Imperial College Press: London, 2004.

(4) Soler-Illia, G. J. A. A.; Sanchez, C.; Lebeau, B.; Patarin, J. Chemical Strategies To Design Textured Materials: From Microporous and Mesoporous Oxides to Nanonetworks and Hierarchical Structures. *Chem. Rev.* **2002**, *102*, 4093−4138.

(5) Soler-Illia, G. J. A. A.; Louis, A.; Sanchez, C. Synthesis and Characterization of Mesostructured Titania-Based Materials through Evaporation-Induced Self-Assembly. *Chem. Mater.* **2002**, *14*, 750−759.

(6) Arconada, N.; Castro, Y.; Durán, A.; Héquet, V. Photocatalytic Oxidation of Methyl Ethyl Ketones Over Sol−Gel Mesoporous and Meso-Structured TiO_2 Films Obtained by EISA Method. *Appl. Catal., B* **2011**, *107*, 52−58.

(7) Milsom, E. V.; Bond, A. M.; O'Mullane, A. P.; Elton, D.; Lee, C. Y.; Marken, F. Probing Second Harmonic Components of pH-Sensitive Redox Processes in a Mesoporous TiO_2-Nafion Film Electrode with Fourier-Transformed Large-Amplitude Sinusoidally Modulated Voltammetry. *Electroanalysis* **2009**, *21*, 41−47.

(8) Chan, C. C.; Chang, C. C.; Hsu, W. C.; Wang, S. K.; Lin, J. Photocatalytic Activities of Pd-Loaded Mesoporous TiO_2 Thin Films. *Chem. Eng. J.* **2009**, *152*, 492−497.

(9) Bellino, M. G.; Tropper, I.; Duran, H.; Regazzoni, A. E.; Soler-Illia, G. J. A. A. Polymerase-Functionalized Hierarchical Mesoporous Titania Thin Films: Towards a Nanoreactor Platform for DNA Amplification. *Small* **2010**, *6*, 1221−1225.

(10) Grinis, L.; Kotlyar, S.; Rühle, S.; Grinblat, J.; Zaban, A. Conformal Nano-Sized Inorganic Coatings on Mesoporous TiO_2 Films for Low-Temperature Dye-Sensitized Solar Cell Fabrication. *Adv. Funct. Mater.* **2010**, *20*, 282−288.

(11) Soler-Illia, G. J. A. A.; Angelome, P. C.; Fuertes, M. C.; Grosso, D.; Boissiere, C. Critical Aspects in the Production of Periodically Ordered Mesoporous Titania Thin Films. *Nanoscale* **2012**, *4*, 2549−2566.

(12) Roncaroli, F.; Blesa, M. A. Kinetics of Adsorption of Carboxylic Acids onto Titanium Dioxide. *Phys. Chem. Chem. Phys.* **2010**, *12*, 9938−9944.

(13) Roncaroli, F.; Blesa, M. A. Kinetics of Adsorption of Oxalic Acid on Different Titanium Dioxide Samples. *J. Colloid Interface Sci.* **2011**, *356*, 227−233.

(14) Araujo, P. Z.; Morando, P. J.; Martínez, E.; Blesa, M. A. Time Evolution of Surface Speciation During Heterogeneous Photocatalysis: Gallic Acid on Titanium Dioxide. *Appl. Catal., B* **2012**, *125*, 215−221.

(15) Hug, S. J.; Sulzberger, B. In Situ Fourier Transform Infrared Spectroscopic Evidence for the Formation Of Several Different Surface Complexes of Oxalate on TiO_2 in the Aqueous Phase. *Langmuir* **1994**, *10*, 3587−3597.

(16) Young, A. G.; McQuillan, A. J. Adsorption/Desorption Kinetics from ATR-IR Spectroscopy. Aqueous Oxalic Acid on Anatase TiO_2. *Langmuir* **2009**, *25*, 3538−3548.

(17) Weisz, A. D.; García Rodenas, L.; Morando, P. J.; Regazzoni, A. E.; Blesa, M. A. FTIR Study of the Adsorption of Single Pollutants and Mixtures of Pollutants onto Titanium Dioxide in Water: Oxalic and Salicylic Acids. *Catal. Today* **2002**, *76*, 103−112.

(18) Weisz, A. D.; Regazzoni, A. E.; Blesa, M. A. ATR-FTIR Study of the Stability Trends of Carboxylate Complexes Formed on the Surface of Titanium Dioxide Particles Immersed in Water. *Solid State Ionics* **2001**, *143*, 125−130.

(19) Regazzoni, A. E.; Mandelbaum, P.; Matsuyoshi, M.; Schiller, S.; Bilmes, S. A.; Blesa, M. A. Adsorption and Photooxidation of Salicylic Acid on Titanium Dioxide: A Surface Complexation Description. *Langmuir* **1998**, *14*, 868−874.

(20) Mendive, C. B.; Bredow, T.; Feldhoff, A.; Blesa, M. A.; Bahnemann, D. Adsorption of Oxalate on Anatase (100) and Rutile (110) Surfaces in Aqueous Systems: Experimental Results vs. Theoretical Predictions. *Phys. Chem. Chem. Phys.* **2009**, *11*, 1794−1808.

(21) Crepaldi, E. L.; Soler-Illia, G. J. A. A.; Grosso, D.; Cagnol, F.; Ribot, F.; Sanchez, C. Controlled Formation of Highly Organized Mesoporous Titania Thin Films: From Mesostructured Hybrids to Mesoporous Nanoanatase TiO_2. *J. Am. Chem. Soc.* **2003**, *125*, 9770−9786.

(22) Crepaldi, E. L.; Soler-Illia, G. J. A. A.; Grosso, D.; Sanchez, C. Nanocrystallised Titania and Zirconia Mesoporous Thin films Exhibiting Enhanced Thermal Stability. *New J. Chem.* **2003**, *27*, 9−13.

(23) Sánchez, V. M.; Martínez, E. D.; Martinez-Ricci, M. L.; Troiani, H. E.; Soler-Illia, G. J. A. A. Optical Properties of Au Nanoparticles Included in Mesoporous TiO_2 Thin Films: A Dual Experimental and Modeling Study. *J. Phys. Chem. C* **2013**, *117*, 7246−7259.

(24) Revol, P.; Perret, D.; Bertin, F.; Fusalba, F.; Rouessac, V.; Chabli, A.; Passemard, G.; Ayral, A. Porosimetry Measurements on Low Dielectric Constant—Thin Layers by Coupling Spectroscopic Ellipsometry and Solvent Adsorption-Desorption. *J. Porous Mater.* **2005**, *12*, 113−121.

(25) Boissiere, C.; Grosso, D.; Lepoutre, S.; Nicole, L.; Bruneau, A. B.; Sanchez, C. Porosity and Mechanical Properties of Mesoporous Thin Films Assessed by Environmental Ellipsometric Porosimetry. *Langmuir* **2005**, *21*, 12362−12371.

(26) Angelomé, P. C.; Andrini, L.; Calvo, M. E.; Requejo, F. G.; Bilmes, S. A.; Soler-Illia, G. J. A. A. Mesoporous Anatase TiO_2 Films: Use of Ti K XANES for the Quantification of the Nanocrystalline

693 Character and Substrate Effects in the Photocatalysis Behavior. *J. Phys.*
694 *Chem. C* **2007**, *111*, 10886−10893.
695 (27) Zhang, Y.; Li, J.; Wang, J. Substrate-Assisted Crystallization and
696 Photocatalytic Properties of Mesoporous TiO_2 Thin Films. *Chem.*
697 *Mater.* **2006**, *18*, 2917−2923.
698 (28) Sakatani, Y.; Grosso, D.; Nicole, L.; Boissiere, C.; de A. A. Soler-
699 Illia, G. J.; Sanchez, C. Optimized Photocatalytic Activity of Grid-Like
700 Mesoporous TiO_2 Films: Effect of Crystallinity, Pore Size Distribution,
701 and Pore Accessibility. *J. Mater. Chem.* **2006**, *16*, 77−82.
702 (29) Violi, I. L.; Pérez, M. D.; Fuertes, M. C.; Soler-Illia, G. J. A. A.
703 Highly Ordered, Accessible and Nanocrystalline Mesoporous TiO_2
704 Thin Films on Transparent Conductive Substrates. *ACS Appl. Mater.*
705 *Interfaces* **2012**, *4*, 4320−4330.
706 (30) Fuertes, M. C.; Marchena, M.; Marchi, M. C.; Wolosiuk, A.;
707 Soler-Illia, G. J. A. A. Controlled Deposition of Silver Nanoparticles in
708 Mesoporous Single or Multilayer Thin Films: From Tuned Pore
709 Filling to Selective Spatial Location of Nanometric Objects. *Small*
710 **2009**, *5*, 272−280.
711 (31) Angelomé, P. C.; Soler-Illia, G. J. A. A. Organically Modified
712 Transition-Metal Oxide Mesoporous Thin Films and Xerogels. *Chem.*
713 *Mater.* **2004**, *17*, 322−331.
714 (32) Rodríguez, R.; Blesa, M. A.; Regazzoni, A. E. Surface
715 Complexation at the TiO_2(anatase)/Aqueous Solution Interface:
716 Chemisorption of Catechol. *J. Colloid Interface Sci.* **1996**, *177*, 122−
717 131.
718 (33) Liu, Y.; Liu, Y. J. Biosorption Isotherms, Kinetics and
719 Thermodynamics. *Sep. Purif. Technol.* **2008**, *61*, 229−242.
720 (34) Azizian, S.; Bashiri, H. Adsorption Kinetics at the Solid/Solution
721 Interface: Statistical Rate Theory at Initial Times of Adsorption and
722 Close to Equilibrium. *Langmuir* **2008**, *24*, 11669−11676.
723 (35) Azizian, S. Kinetic Models of Sorption: A Theoretical Analysis. *J.*
724 *Colloid Interface Sci.* **2004**, *276*, 47−52.
725 (36) Plazinski, W.; Rudzinski, W. Kinetics of Adsorption at Solid/
726 Solution Interfaces Controlled by Intraparticle Diffusion: A Theoreti-
727 cal Analysis. *J. Phys. Chem. C* **2009**, *113*, 12495−12501.
728 (37) Rudzinski, W.; Plazinski, W. Studies of the Kinetics of Solute
729 Adsorption at Solid/Solution Interfaces: On the Possibility of
730 Distinguishing between the Diffusional and the Surface Reaction
731 Kinetic Models by Studying the Pseudo-First-Order Kinetics. *J. Phys.*
732 *Chem. C* **2007**, *111*, 15100−15110.
733 (38) Liu, Y.; Shen, L. From Langmuir Kinetics to First- and Second-
734 Order Rate Equations for Adsorption. *Langmuir* **2008**, *24*, 11625−
735 11630.
736 (39) Takahashi, R.; Sato, S.; Sodesawa, T.; Nishida, H. Effect of Pore
737 Size on the Liquid-Phase Pore Diffusion of Nickel Nitrate. *Phys. Chem.*
738 *Chem. Phys.* **2002**, *4*, 3800−3805.
739 (40) Araujo, P. Z.; Luca, V.; Bozzano, P. B.; Bianchi, H. L.; Soler-Illia,
740 G. J. A. A.; Blesa, M. A. Aerosol-Assisted Production of Mesoporous
741 Titania Microspheres with Enhanced Photocatalytic Activity: The
742 Basis of an Improved Process. *ACS Appl. Mater. Interfaces* **2010**, *2*,
743 1663−1673.